Indian Journal of Pure & Applied Physics
Vol. 59, December 2021, pp. 850-856

Photoluminescence Study of Up-Conversion Phosphor $La_2(MoO_4)_3$ Yb^{3+}, Er^{3+} Prepared by Precipitation Method

Kevil Shah, Sohan M Chauhan* & B S Chakrabarty

Luminescence Lab, Applied Physics Department, Faculty of Technology & Engineering,
The Maharaja Sayajirao University of Baroda, Vadodara, Gujarat, 390 002, India.

Received 19 July 2019; accepted 1 November 2021

Up-conversion phosphors of $La_2(MoO_4)_3$: Yb^{3+}, Er^{3+} with different concentration of Erbium were prepared by a simple precipitation method. The crystal structure, surface morphology, elemental composition and photoluminescence properties were characterized by X–ray powder diffraction (XRD), Scanning electron microscopy (SEM), Energy dispersive X–ray Spectroscopy (EDAX) and Photoluminescence spectroscopy respectively. XRD spectra show high degree of crystallinity in all samples. SEM images shows rod like structures presence in the samples. EDAX analysis confirm the presence of dopants (Yb^{3+} and Er^{3+}) in the host matrix ($La_2(MoO_4)_3$). Upon excitation by 980 nm infrared radiation, all the samples give emission peaks between 524 – 533 nm in the bluish green region, 546 – 555 nm in the green region and 659 – 672 nm in the red region which are attributed to the $^2H_{11/2} \rightarrow {}^4I_{15/2}$, $^4S_{3/2} \rightarrow {}^4I_{15/2}$ and $^4F_{9/2} \rightarrow {}^4I_{15/2}$ transitions of Er^{3+} ions respectively.

Keywords: Up-conversion process, Phosphor, Photoluminescence, Precipitation, Chromaticity, Up-conversion mechanism, Energy transitions

1 Introduction

Every new efficient lighting technologies depends on rare-earth materials, these materials serves as host or as dopant in lighting or display device industries[1-2]. The every element in rare-earth family has same chemical properties but has different physical properties because of their electronic structure (outer cell)[3-5]. Because of these unique structures, they have ability to give sharp emission and this makes them use in display and lighting technologies[6-8]. In recent development of imagine technique, these metals act as biological probe[9]. There has been a lot of interest in rare earth doped luminescent materials due to their applications in various field such as solid-state lasers, phosphors, optoelectronics, bio imaging, biolabeling, etc. One of the important segments in these materials are the up-conversion phosphors because of their ability to convert two or more lower energy photons in the near infrared region to a higher energy photon in the visible region[10-11]. This type of conversion process is very important in the biological application because it offers features like improved light penetration depth, high chemical and photo stability, absence of auto-fluorescence during imaging, high resistance to photo bleaching and sharp emission bands[12]. These types of characteristics may overcome the limitations which are present in the traditional luminescent materials. The rare earth ions are characterized by the sharp emission lines in the optical spectrum due to their filled 4f shell and the associated shielding by 5s and 5p orbitals. The rare earth ions as activators in a rare earth host matrix can easily replace each other owing to their similar properties in terms of both the valance state and ionic size[13-14].

Rare earth doped molybdates have promising applications in the field of optical fibers, laser host materials, phosphors, etc. Among the various rare earth doped molybdates, a promising host candidate for luminescent material is Lanthanum Molybdate ($La_2(MoO_4)_3$)[15]. There are several forms of lanthanum molybdate such as $La_2(MoO_4)_3$ (monoclinic), La_2MoO_8 (monoclinic), $La(Mo_8O_{14})$ (orthorhombic), $La_2O_2(MoO_4)$ (tetragonal), $La_2Mo_2O_9$ (cubic), La_6MoO_{12} (rhombohedral), $La_6Mo_2O_{14}$ (hexagonal), La_2MoO_6(tetragonal), $La_6Mo_2O_{15}$ (orthorhombic), etc. Several methods like solid-state, sol-gel, hydrothermal, etc. have been used to synthesize lanthanum molybdates[16-20]. However, to the best of our knowledge, there is no report of the synthesis of $La_2(MoO_4)_3$: Yb^{3+}, Er^{3+} by precipitation method. This reported method for the synthesis of Lanthanum Molybdate is unique synthesis technique which has consume less time for process and gives high amount

*Corresponding author:
(E-mail: smchauhan.msu@gmail.com)

of yield thus become ecofriendly and industrial friendly.

2 Materials and method

$La_2(MoO_4)_3$: Yb^{3+}, Er^{3+} phosphor samples were synthesised to study their up-conversion characteristics by a simple and cost effective precipitation method with three different concentration of Erbium content (1, 2 and 3 mol%). Three samples were synthesized in the following proportion of the host metal ($La_2(MoO_4)_3$), the sensitizer (Yb^{3+}) and activator (Er^{3+}) as (La:Yb: Er = 79:20:1, 78:20:2 and 77:20:3) and labeled them as LMO 1, LMO 2 and LMO 3 respectively.

The rare earth based raw materials Lanthanum Oxide (La_2O_3), Ytterbium Oxide (Yb_2O_3) and Erbium Oxide (Er_2O_3) were procured from Sigma-Aldrich.

Stoichiometric amount of Lanthanum Oxide (La_2O_3), Ytterbium Oxide (Yb_2O_3) and Erbium Oxide (Er_2O_3) were taken and dissolved in 10 ml of dilute HNO_3 to prepare Solution A. The solution was heated moderately to drive away the unreacted HNO_3. The residue obtained was dissolved in 30 ml of deionised water and stirred for one hour at room temperature. Another mixture (Solution B) was prepared by dissolving stoichiometric amount of Ammonium Molybdate Oxide ($(NH_4)_6Mo_7O_{24}$) in 30 ml of deionised water and stirring it for one hour at room temperature. Solution A was added to Solution B drop by drop and the mixture was stirred continuously for 24 hours. Gradually, the precipitates were formed. These precipitates were then centrifuged at 3000 rpm for 15 minutes, washed twice in deionised water and dried. The color of the precipitates was light green like that of bottle gourd. These precipitates were heated at 800 ºC for 5 hours and then cooled. The final product was a light lemon colored powder.

3 Results and discussion

The samples were characterized by X – ray powder diffraction technique using X'Pert Pro PAN aytical Powder Diffract meter with Cu-Kα radiation source (λ = 1.54 Å) operated at 40 kV and 40 mA in the 2Θ range 20 – 80 degree at the scan speed of 0.05 degree per second. The morphology and elemental composition detection was carried out by Energy Dispersive X–ray Spectroscopy (EDAX) system equipped with a Scanning Electron Microscope (JEOL make MODEL JSM 5810 LV). The up-conversion photoluminescence study for this work was carried out by using confocal photoluminescence mapping system (alpha 300 M+) – WItec Co. at National Physical Laboratory, Delhi. In this system, the excitation source of 150 W Xenon arc lamp is replaced by a 980 nm infrared laser diode. The I – V characteristics of the samples were carried out by simple set up made in the laboratory.

3.1 X-ray Powder Diffraction analysis

Fig. 1 shows the XRD pattern for sample LMO 1 ($La_2(MoO_4)_3$:Yb^{3+}, Er^{3+}), which has sharp peaks. The pattern indicates high degree of crystallinity. These peaks can be ascribed to $La_2(MoO_4)_3$. The structure is predominantly in monoclinic phase. The peak at 2Θ value of 25.85º has the highest intensity, which is the characteristic peak of (-421) plane. d-values of majority of the peaks match with those reported in the JCPDS file (70 – 1382) for $La_2(MoO_4)_3$, while a few vary marginally with the respective peaks in the same file. That can be attributed to the presence of dopants. Figs. 2 & 3 show similar pattern for the other two samples. Some peaks match with JCPDS file no. 78 – 1691 of Yb_2O_3 and 76 – 0159 for Er_2O_3 which shows that there is some amount of residual Yb_2O_3 and Er_2O_3 in the samples.

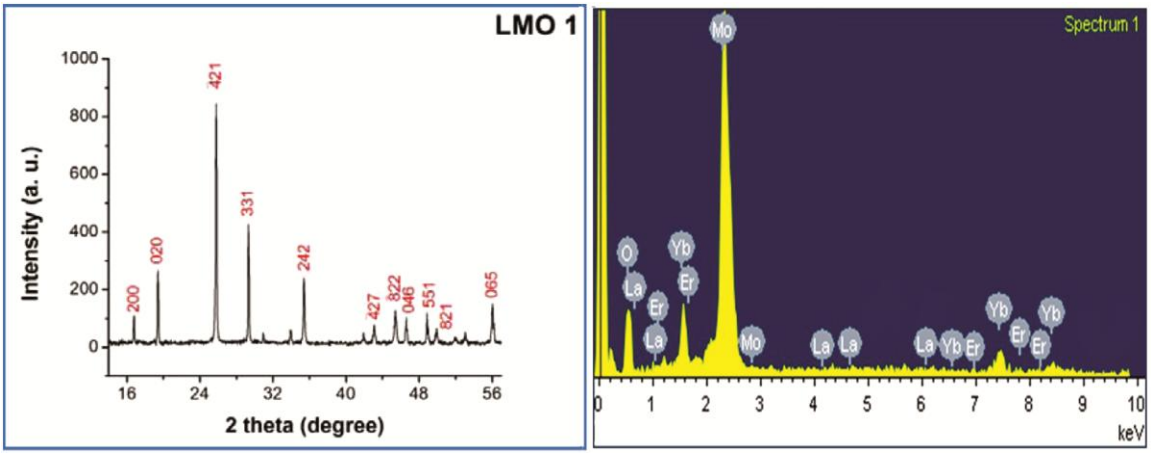

Fig. 1 — XRD and EDAX results of LMO 1

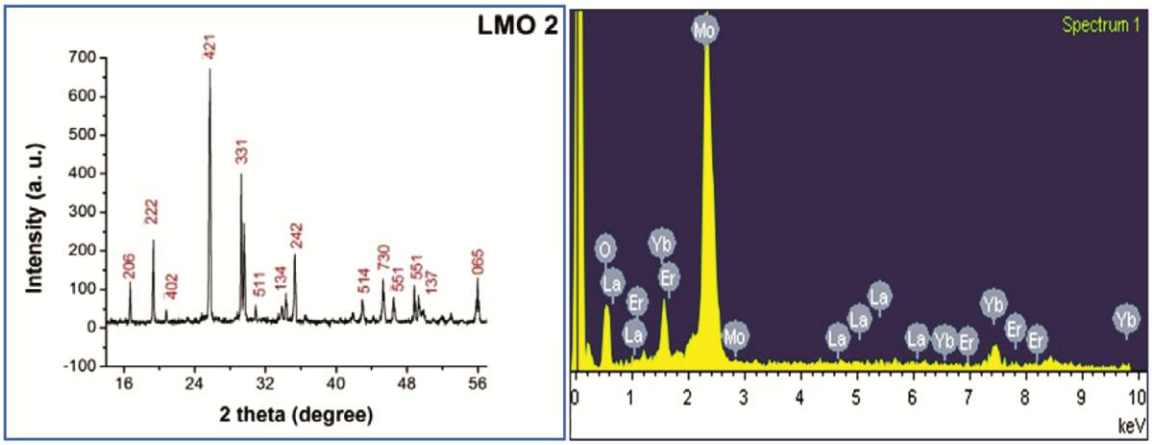

Fig. 2 — XRD and EDAX results of LMO 2

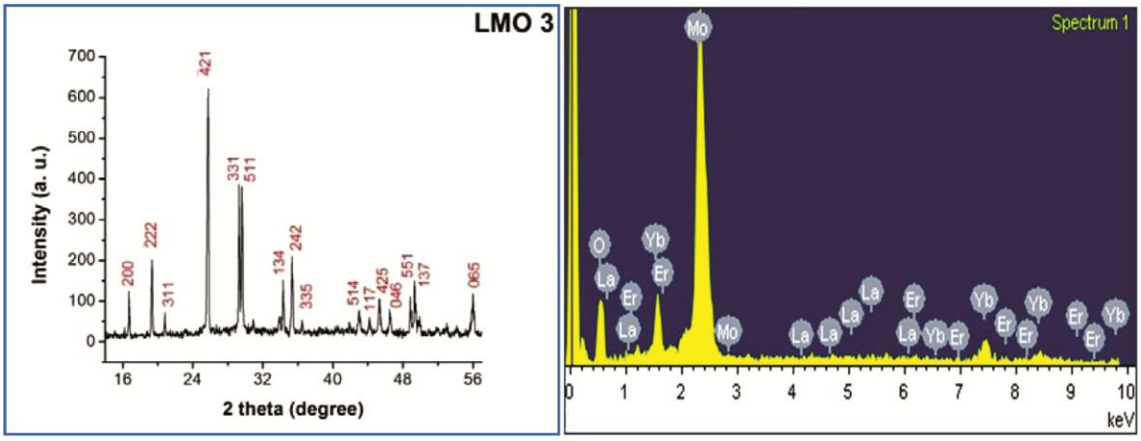

Fig. 3 — XRD and EDAX results of LMO 3

Table 1 — Crystallite size for samples of $La_2(MoO_4)_3$: Yb, Er

Sample Name	Crystallite Size (nm)
LMO 1	61.79
LMO 2	69.13
LMO 3	74.07

The average crystallite size was calculated by Debye – Scherrer formula. The values are given in Table 1. From the table 1, it can be seen that with increase in the Erbium content, crystallite size of the samples also increases.

3.2 Energy Dispersive X – ray Spectroscopy (EDAX) analysis

The samples were subjected to EDAX analysis to confirm the presence of elements, particularly the doped elements in the samples. The results confirm the presence of all the elements involved (see the Figs. 1, 2 & 3).

3.3 Scanning Electron Microscopy (SEM) analysis

The images for sample LMO 1, LMO 2 and LMO 3 are given in Figs. 4, 5 & 6 respectively at 2000 X magnification. The images show coarse grain structure with a large variation of grain size and aggregation. In Figs. 5 & 6, large chunks can be seen which look like aggregated grains of rod like structures.

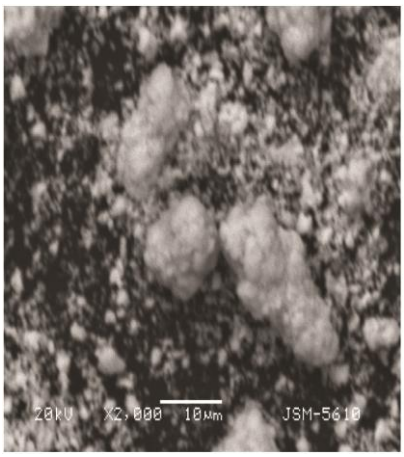

Fig. 4 — SEM image of sample LMO 1

It can be suggested that the presence of Erbium is instrumental in the samples acquiring the rod shape.

However, the host material also plays a role in determining the shape. It is also guided by the method of synthesis.

3.4 Up-conversion characteristics

The up-conversion characteristics of the synthesized samples were recorded using a set up with an excitation source of 980 nm. Similar amount of sample was taken for each of the recording. Figs. 7, 8 & 9 show the emission spectra of the samples for excitation at 980 nm.

Sample LMO 1 as shown in Fig. 7 gives strong emission at 523, 527 and 533 nm in the bluish green region as well as 547 and 555 nm in the green region. There are minor peaks at wavelengths 644, 659 and 671 nm in the red region. The peaks in the green region only contribute to the intensity as the intensity of peaks in the red region is insignificant. Other two samples give similar results with minor change in the spectral positions but significant changes in the relative intensities.

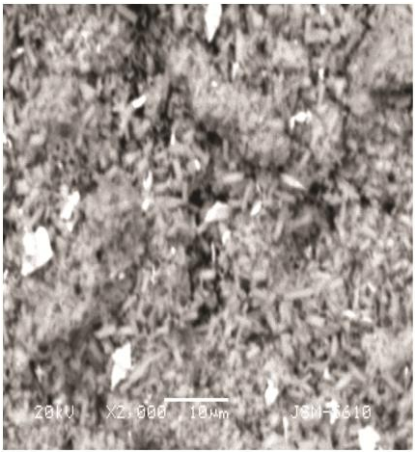

Fig. 5 — SEM image of sample LMO 2

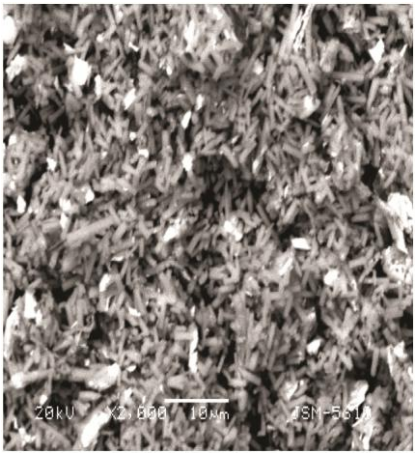

Fig. 6 — SEM image of sample LMO 3

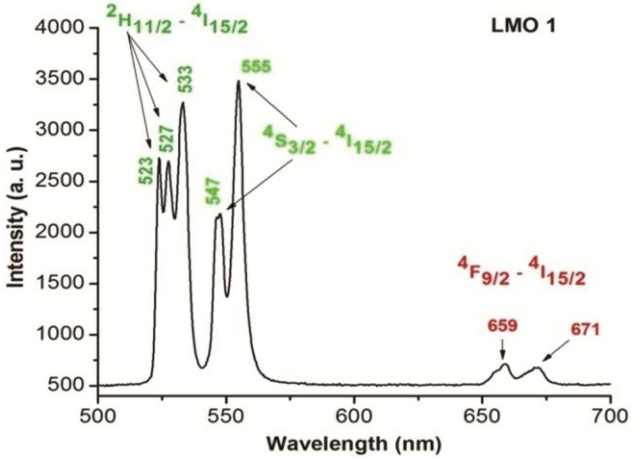

Fig. 7 — Emission spectrum of sample LMO 1

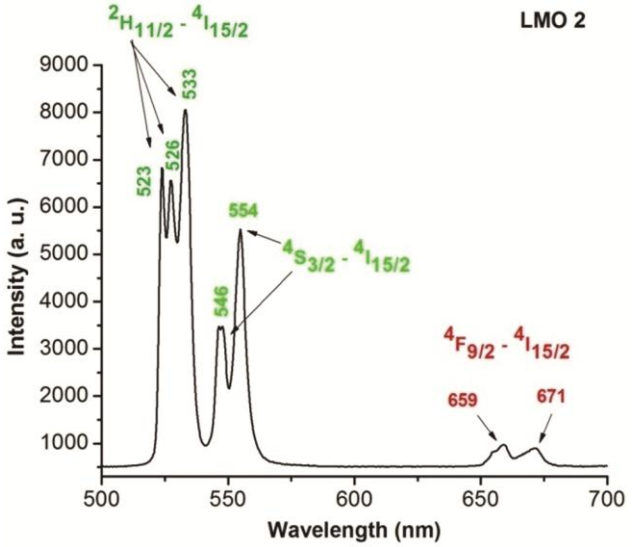

Fig. 8 — Emission spectrum of sample LMO 2

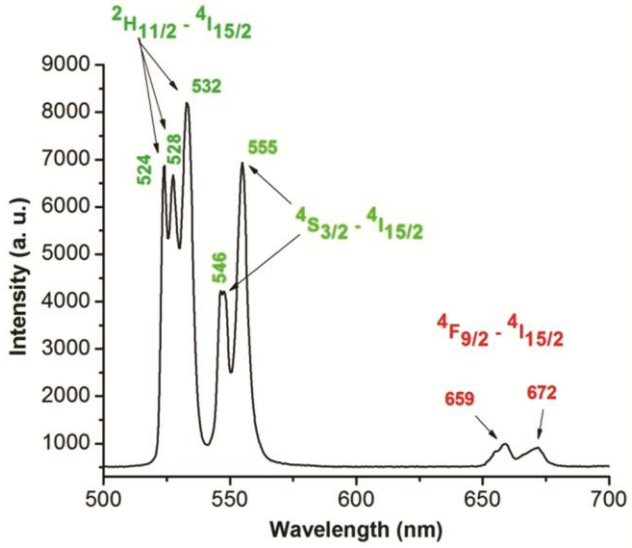

Fig. 9 — Emission spectrum of sample LMO 3

The peaks in the bluish green region are attributed to the transition $^2H_{11/2} \rightarrow {}^4I_{15/2}$ of Er^{3+}ion, while those in the green region are attributed to the transition $^4S_{3/2} \rightarrow {}^4I_{15/2}$ of the same ion[21-22]. Peaks in the red region are of $^4F_{9/2} \rightarrow {}^4I_{15/2}$ transition of Er^{3+}. The free Er^{3+} ion would have an electron configuration $4f^{11}$. The lower term corresponding to this configuration is $^4I_{15/2}$. However, in the presence of crystal field, this level degenerates due to stark splitting giving multiple peaks for the transitions mentioned above. This explains the multiplicity of peaks for each transition.

The changes in intensity of the peaks in all the three samples show a general trend as shown in Fig. 10. It shows that there is increase in intensity of the peaks with increase in the amount of Erbium. At lower concentration of Erbium (sample LMO 1), the transition $^4S_{3/2} \rightarrow {}^4I_{15/2}$ dominates as the intensity of the 555 nm peak is higher than the 533 nm peak of transition $^2H_{11/2} \rightarrow {}^4I_{15/2}$. However, at higher concentrations of Erbium (samples LMO 2 and LMO 3), the transition $^2H_{11/2} \rightarrow {}^4I_{15/2}$corresponding to 533 nm clearly dominates over the other. Intensities due to the $^4F_{9/2} \rightarrow {}^4I_{15/2}$transition in the red region do not show any significant change.

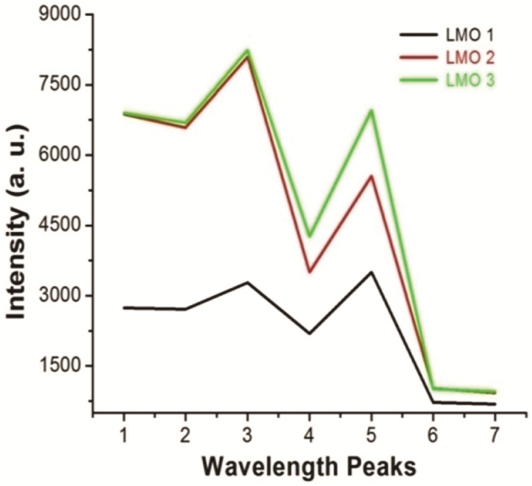

Fig. 10 — Change in peak intensities

Fig 11(a) & 11(b) show that the intensities of the peaks attributed to the transition $^2H_{11/2} \rightarrow {}^4I_{15/2}$ get saturated on increase in the Erbium content, while the intensities of the peaks attributed to the transition $^4S_{3/2} \rightarrow {}^4I_{15/2}$ increase almost linearly. In general, it is seen that by increasing the concentration of Erbium, there is an increase in the intensity of the emission peaks for green color emission[23-24].

Up-conversion mechanism in $La_2(MoO_4)_3$: Yb^{3+}, Er^{3+}

Based on the emission characteristics, the up-conversion mechanism in $La_2(MoO_4)_3$: Yb, Er can be described, which is shown in Fig. 12.

The 980 nm radiation is absorbed by the Yb^{3+} ions, as they have a much higher absorption cross section. It results in excitation of the Yb^{3+} ions from $^2F_{7/2} \rightarrow {}^2F_{5/2}$. The de-excitation of Yb^{3+} ion from $^2F_{5/2} \rightarrow {}^2F_{7/2}$ leads to generation of photons with energy equal to the difference in energy levels, $^4I_{11/2}$ & $^4I_{15/2}$ as well as $^4F_{7/2}$ & $^4I_{11/2}$ of Er^{3+} ions. In the next step, there is **Energy Transfer (ET)** of the energy generated as mentioned above, from Yb^{3+} ions (the sensitizer), to the Er^{3+} ions (the activator) in two different ways. First, Energy transferred to Er^{3+} ions resulting in **Ground State Absorption (GSA)** in the Er^{3+} ion, which leads to excitation of these ions from $^4I_{15/2} \rightarrow {}^4I_{11/2}$. Second, Energy transferred to Er^{3+} ions resulting in **Excited State Absorption (ESA)** in the Er^{3+} ion, which leads to excitation of these ions from $^4I_{11/2} \rightarrow {}^4F_{7/2}$. The electrons get accumulated at the $^4F_{7/2}$ level of Er^{3+} ion. Some of the electrons accumulated at the $^4F_{7/2}$ level release some energy non radiatively and reach $^2H_{11/2}$ level, from where their transition to the $^4I_{15/2}$ level results into the bluish green emission of the three peaks (523, 527 and 533 nm) **{ $^2H_{11/2} \rightarrow {}^4I_{15/2}$ }.**

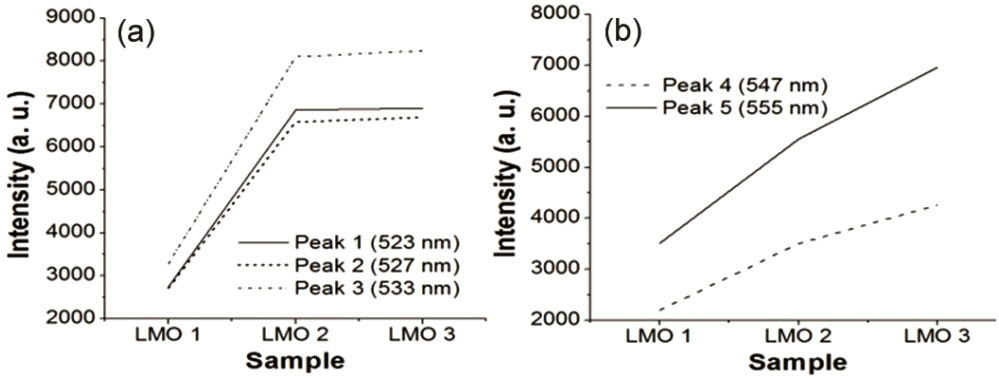

Fig. 11(a,b) — Change in peak intensity for the transition

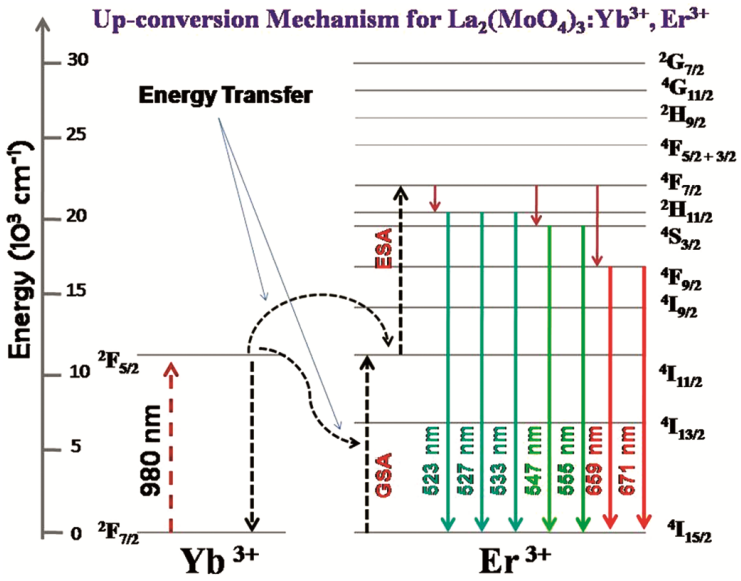

Fig. 12 — Mechanism of up conversion in $La_2(MoO_4)_3$: Yb^{3+}, Er^{3+}

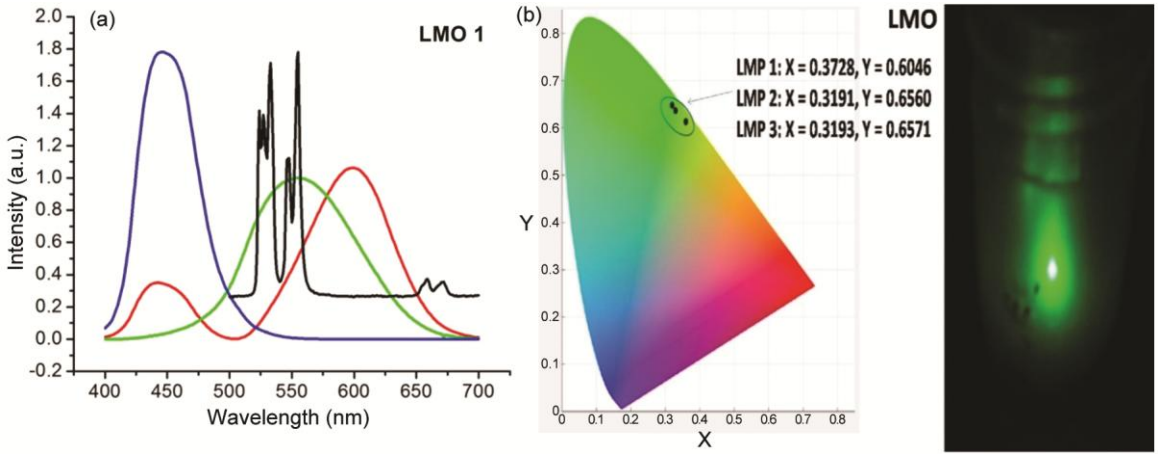

Fig. 13(a-b) — Chromaticity Diagram; (b) —— Color matching Function and photograph

Other electrons release more energy by non radiative transitions to reach $^4S_{3/2}$ level. Their transition to the $^4I_{15/2}$ level results into the emission of the two peaks (547 and 555 nm) **{ $^4S_{3/2} \rightarrow {}^4I_{15/2}$ }.** Few of these electrons release further energy at the $^4S_{3/2}$ level by non radiative means to reach the $^4F_{9/2}$ level. These electrons transit to the $^4I_{15/2}$ level to give emission in the red region **{ $^4F_{9/2} \rightarrow {}^4I_{15/2}$ }**[25-28].

4 Chromaticity Diagram

The colour emitted by a phosphor can be visualized and understood by its position in the chromaticity diagram. For obtaining this position in terms of chromaticity coordinates, the emission characteristics of the samples were superimposed with the colour matching functions. Colour matching functions are the amounts of primary colours needed to match a particular colour. These primary colours have been standardized by CIE in 1931 as the RGB colour matching functions r(λ), g(λ) and b(λ) corresponding to 700 nm, 546.1 nm and 435.8 nm respectively in the red, green and blue regions of the spectrum. The overlap between the emission spectra and the respective colour matching functions give the chromaticity coordinates of the emitted colour. An illustration has been given in Fig. 13(a) for sample LMO1. The chromaticity coordinates are marked in Fig. 13(b) in the small oval for all the samples along with the photograph of light emission[29].

5 Conclusion

$La_2(MoO_4)_3$: Yb^{3+}, Er^{3+} up-conversion phosphor samples have been prepared by the simple precipitation method. XRD analysis of the samples

shows high degree of crystallinity. They are in monoclinic phase. Crystallite size of the samples increases as the Erbium content increases. EDAX analysis of the samples confirms the presence of the activator (Er3+) and sensitizer (Yb3+) as well as all elements of the host matrix ($La_2(MoO_4)_3$).SEM images of $La_2(MoO_4)_3$ show coarse grain structure with large variation in grain size. Higher resolution images show aggregation of rod like structures. The samples give major emissions in the green and some emission in the red region. The emission with multiple peaks is attributed to the Er^{3+} ions, while Yb^{3+} acts as a sensitizer. There is splitting of peaks in the bluish green and green regions on account of the stark effect due to the crystal field of the host material. An increase in intensity is observed in the green region with increase in the Erbium content.

Acknowledgement

We are thankful to UGC – NEW DELHI for providing the UGC – BSR – RFSMS Fellowship.

References

1 Tessler N, Medvedlv V & Kazes M, *Science*, 295 (2002) 1506.
2 Chan W C W & Nie S, *Science*, 281(1998) 2016.
3 Fessari M, *Nat Rev*, 5 (2005) 161.
4 Medintz E L, Trammell S A & Mattoussi H, *J Am Chem Soc*, 126 (2004) 30.
5 Selvan S T, Patra P K & Ang C Y, *Chem. Int. Ed. Engl*, 46 (2007) 2448.
6 Cho S J, Maysinger D, Jain M & Roder B, *Langmuier*, 23 (2007) 1974.
7 Li J, Bu W, Guo L & Chen Z, *J Mater Res*, 23 (2008) 16.
8 Mednintz I L, Vyeda H T & Goldman E R, *Nat Mater*, 4 (2005) 435.
9 Michalet X, Pinaud F F, Bentolila L A & Tsay J M, *Science*, 307 (2005) 538.
10 Wang F, Tan W B & Zhang Y, *Nanotechnology*, 17 (2006) 1-13.
11 Gordon W O, Carter J A & Tissue B M, *J Lumin*, 108 (2004) 339.
12 Feng Wang, Banerjee D, Liu Y & Chen X, *Analyst*, 135 (2010) 1839.
13 Xie R J, Mitomo M & Uheda K, *J Am Ceram Soc*, 85 (2002) 1229.
14 Maestro P & Huguenin D, *J Alloys Compd*, 225 (1995) 520.
15 Chang S L, *Anal Sci Technol*, 6 (2014) 314.
16 Chen Z, Bu W & Zhang N, *J Phys Chem C*, 112 (2008) 4378.
17 G Yi, Sun B & Yeng F, *Chem Mater*, 14 (2002) 2910.
18 Zhang N, Bu W & Xu Y, *J Phys Chem C*, 111 (2007) 5014.
19 Zhiyi G, Zhiying W & Linlin Fu, *Mater Res Bullet*, 70 (2015) 779.
20 Bissengaliyeva M R, Bekturganov N S & Gogol D B, *Mater Chem Phys*, xxx (2015) 1.
21 Laachir S, Moussetad M & Adhiri R, *Z. Naturforsch*, 66a (2011) 457.
22 Tyagi N, Reddy A A & Nagarajan R, *Opt Mater*, 33 (2010) 42.
23 Zou H, Li J, Cao Q & Wang X, *J Adv Dielectr*, 4 (2014) 1450028.
24 Guo H, Qiao Y, Zheng J & Zhao L, *Chinese J Chem Phys*, 21 (2008) 233.
25 Guo H, *J Solid State Chem*, 180 (2007) 127.
26 Wang Y & Ohwaki J, *J Appl Phys*, 74 (1993) 1272.
27 Ciric A, Shah K & Sekulic M, *Optik*, 245 (2021) 167690.
28 Ciric A, Sekulic M & Shah K, *Opt Mater*, 120 (2021) 111417.
29 Fairman H S, Brill M H & Hemmendinger H, *Color Res Appl*, 22 (1997) 11.